ELSEVIER

Journal of Organometallic Chemistry 633 (2001) 91–104

Journal of Organometallic Chemistry

www.elsevier.com/locate/jorganchem

Polymorphism and metal–metal interactions on $[Rh(Cl)(CO)_2(Hpz^R)]$ complexes

M.C. Torralba [a], M. Cano [a,*], J.A. Campo [a], J.V. Heras [a], E. Pinilla [a,b], M.R. Torres [b]

[a] *Departamento de Química Inorgánica I, Facultad de Ciencias Químicas, Universidad Complutense, E-28040 Madrid, Spain*
[b] *Laboratorio de Difracción de Rayos-X, Facultad de Ciencias Químicas, Universidad Complutense, E-28040 Madrid, Spain*

Received 17 April 2001; accepted 1 June 2001

Abstract

The novel pyrazoles containing 3-[4-*n*-hexyloxyphenyl] (hp), 3-[4-*n*-octyloxyphenyl] (op) and 3-[4-*n*-decyloxyphenyl] (dp) substituents, Hpz^R (R = hp, op, dp; **1**–**3**), and their corresponding Rh(I) compounds $[Rh(Cl)(LL)(Hpz^R)]$ (LL = 2,5-norbornadiene NBD, 1,5-cyclooctadiene COD, 2CO; R = hp, op, dp; **4**–**12**) have been prepared and characterised. The influence of the pyrazol substituent on the properties of the Rh(I) complexes has been analysed. Two crystalline polymorphs (yellow and red) have been isolated for $[Rh(Cl)(CO)_2(Hpz^{dp})]$ (**12**) in contrast to the single red crystalline form isolated for the related complexes $[Rh(Cl)(CO)_2(Hpz^R)]$ (R = hp, op; **10** and **11**). X-ray crystal structures of the red forms of **10**–**12** as well as the yellow one of **12** have been solved. The red compounds display one-dimensional stacking of square-planar molecules with metal–metal interactions along the *c*-axis. The yellow form consists of dimeric unities held together by Cl bridges, and without the one-dimensional metal–metal contacts. In both cases an intramolecular hydrogen bond was present, being stronger in the yellow form than in the red one. Thermochromic behaviour has also been observed for these dicarbonyl complexes. No liquid crystals properties were found for the new compounds, however, the double melting behaviour observed for **10**–**12** could be closely related to mesomorphism.

Keywords: Long chain-substituted pyrazoles; Rhodium–pyrazol complexes; Crystalline polymorphism; One-dimensional stacking; Thermochromism

1. Introduction

The study of liquid crystal materials containing transition metals has increased in recent years [1–6]. In this regard, the chemistry of complexes of the nickel triad have been extensively developed and, comparatively in less extension, also iridium and rhodium derivatives. Specifically, the calamitic liquid crystal behaviour of some rod-like complexes of type *cis*-$[M(Cl)(CO)_2(L)]$ (M = Rh, Ir; L = N-donor ligand with extended long-chain substituents) has been well established [3,5,7–13]. It is interesting to note that the complex $[Rh(Cl)(CO)_2(Hpz^{Me2,4R})]$ ($Hpz^{Me2,4R}$ = 4-[(4′-((4″-*n*-decyloxybenzoyl)oxy)phenoxy)carbonyl] - 3,5 - dimethylpyrazole) has recently been described as the first organometallic pyrazol derivative having liquid crystal properties [14]. This behaviour opens new spectatives for the use of extended rod-like pyrazol ligands for generating related metallomesogenic compounds.

Previous work from this laboratory has dealt with Rh(I) complexes of the type *cis*-$[Rh(Cl)(CO)_2(Hpz^{R',R''})]$ (R′ = *t*-Bu, Ph, An, R″ = H; R′ = *t*-Bu, Ph, R″ = Me) containing bulky pyrazol ligands substituted in the 3(5) or 3 and 5 positions and some interesting features have been found depending on the substituents on the pyrazol ring [15]. Although in all cases the colour of complexes in solution was orange–yellow, in the solid state they were found to be blue–black, green–violet or violet, this dark colour being associated with the presence of one-dimensional metal–metal interactions as a consequence of the crystal packing of the square-planar molecules. This arrangement was confirmed through the crystalline structure of the green–violet compound

* Corresponding author. Fax: +34-91-3944352.
E-mail address: mmcano@eucmax.sim.ucm.es (M. Cano).

0022-328X/01/$ - see front matter
PII: S0022-328X(01)01058-0

$[Rh(Cl)(CO)_2(Hpz^{An})]$ which revealed to an intermetallic Rh–Rh distance (3.398(3) Å) slightly shorter than that previously found for $[Rh(Cl)(CO)_2(Hpz)]$ (3.4522(4) Å) which contains a non-substituted pyrazol ligand [16], but 0.13 Å longer than in $[Rh(acac)(CO)_2]$ [17] which has been described as an intrinsic semiconductor [18]. Additionally, the complex $[Rh(Cl)(CO)_2(Hpz^{bp})]$ (Hpz^{bp} = 3-[4-*n*-butoxyphenyl]pyrazole), which was also described for us [19], presented the blue colour characteristic of the previously mentioned metal–metal interactions although no crystals of sufficient quality for X-ray diffraction could be isolated in this case.

The molecular packing in the above complexes consisted of columns defined by stacking of parallel square-planar molecules which were alternatively staggered. The molecules of contiguous columns were oriented in opposite directions, and no short intermolecular contacts between the columns were found. Considering this arrangement it is possible that the introduction of long substituents on the pyrazol groups could give rise to new types of interactions between molecules of contiguous columns as depicted in Fig. 1.

By the extension of these previous results, towards the design of Rh(I) complexes with liquid crystal properties, we have now prepared and studied complexes of the type $[Rh(Cl)(CO)_2(Hpz^R)]$ having pyrazol ligands with long-chain substituents at the 3(5) position. In particular, three new substituted pyrazol ligands 3-(4-*n*-hexyloxyphenyl)pyrazole (Hpz^{hp}) (**1**), 3-(4-*n*-octyloxyphenyl)pyrazole (Hpz^{op}) (**2**) and 3-(4-*n*-decyloxyphenyl)pyrazole (Hpz^{dp}) (**3**), have been synthesised as well as their corresponding complexes $[Rh(Cl)(CO)_2(Hpz^R)]$ (Scheme 1).

The aim of this work is to explore the structural consequences that the changes of the length of the chain of the *n*-alkoxyphenyl group, $C_nH_{2n+1}O$ ($n = 6$, 8, 10), on the pyrazole, would have on the complexes as well as on their potential liquid crystal properties. On this basis, the presence of different crystalline forms and their X-ray structures are analysed and related with the thermal behaviour of the complexes.

2. Experimental

2.1. Materials and physical measurements

All commercial reagents were used as supplied. Syntheses of the starting Rh-complexes $[Rh(\mu\text{-}Cl)(LL)]_2$ (LL = 2,5-norbornadiene NBD, 1,5-cyclooctadiene COD) have been described previously [20,21]. The other starting Rh-complex $[Rh(\mu\text{-}Cl)(CO)_2]_2$ was purchased from Sigma–Aldrich and used as supplied.

The 4-*n*-hexyloxyacetophenone, 4-*n*-octyloxyacetophenone and 4-*n*-decyloxyacetophenone derivatives were synthesised by alkylation of 4-hydroxyacetophenone with the corresponding *n*-alkyliodide in the ace-

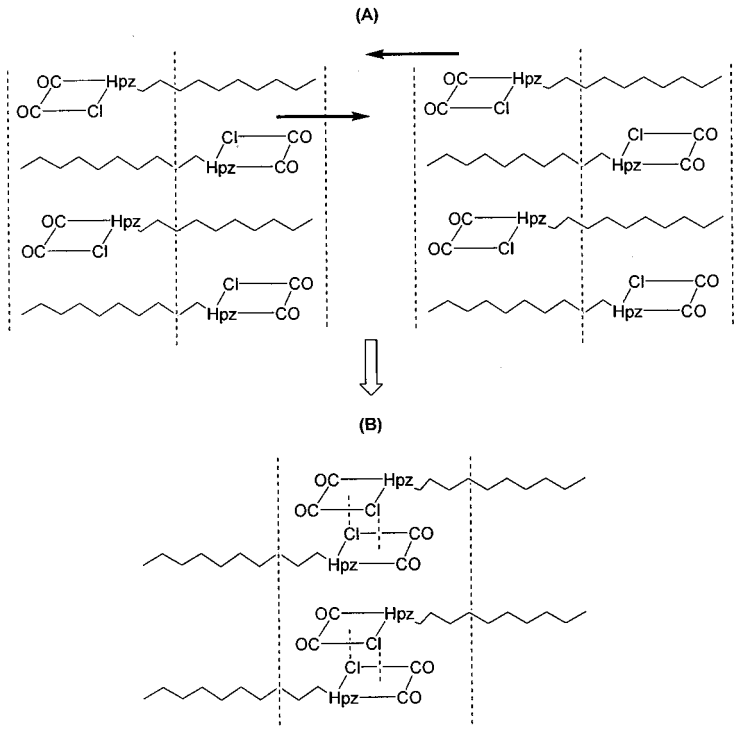

Fig. 1. Intermolecular Cl-bridge interactions (B) suggested on the basis of a molecular gliding (indicated by the arrows) from molecules of adjacent columns (A).

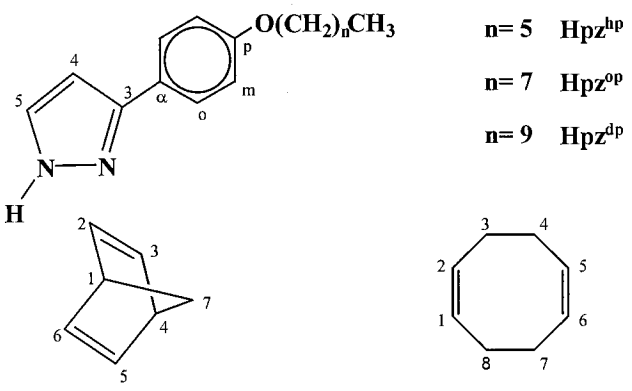

	R	LL	Number
Hpz^R	hp		**1**
	op		**2**
	dp		**3**
$[RhCl(Hpz^R)(LL)]$	hp	NBD	**4**
	op	NBD	**5**
	dp	NBD	**6**
	hp	COD	**7**
	op	COD	**8**
	dp	COD	**9**
	hp	2CO	**10**
	op	2CO	**11**
	dp	2CO	**12**

Scheme 1.

tone solution of K_2CO_3 as previously described for related compounds [22].

Elemental analyses for carbon, hydrogen and nitrogen were carried out by the Microanalytical Service of the Complutense University. IR spectra were recorded on a FTIR Nicolet Magna-550 spectrophotometer with samples as KBr pellets or in CH_2Cl_2 solution in the 4000–350 cm^{-1} region.

^1H- and $^{13}C\{^1H\}$-NMR spectra were performed on a Varian VXR-300 or on a Bruker AM-300 spectrophotometers of the NMR Service of the Complutense University from solutions in $CDCl_3$. Chemical shifts δ are listed in ppm relative to Me_4Si using the signal of the deuterated solvent as reference, and coupling constants J are in Hz. Multiplicities are indicated as s (singlet), d (doublet), t (triplet), q (quintuplet), m (multiplet) and br s (broad signal). The atomic numbering used in the assignment of the NMR signals is shown in Scheme 1. The ^1H- and ^{13}C-NMR chemical shifts are accurate to 0.01 and 0.1 ppm, respectively, and coupling constants are accurate to 0.3 Hz for ^1H-NMR spectra.

The electronic spectra were registered on a CARY 5G spectrophotometer with solutions ca. 10^{-4} M of the complexes in CH_2Cl_2.

Phase studies were carried out by optical microscopy using an Olympus BX50 microscope equipped with a Linkam THMS 600 heating stage. The temperatures were assigned on the basis of optic observations with polarised light.

Measurements of the transition temperatures were made using a Perkin–Elmer Pyris 1 differential scanning calorimeter with the sample (2–6 mg) hermetically sealed in aluminium pans and with a heating or cooling rate of 10 °C min^{-1}.

2.2. Synthetic methods

2.2.1. Preparation of Hpz^R ($R = hp$, op, dp) (**1–3**)

To a solution of the corresponding substituted acetophenone (9.42 mmol) in ethyl formate (18.84 mmol) and toluene (20 ml) was added a slurry of anhydrous sodium methoxide (9.42 mmol) in toluene (30 ml). The reaction mixture was stirred for 24 h at room temperature (r.t.). The solid formed was isolated by filtration and washed with CH_2Cl_2 and hexane.

The solid was dissolved in MeOH (30 ml) and hydrazine chlorhydrate (9.42 mmol) in water (10 ml) was added very slowly. The solution was stirred for 12 h at r.t., then the solvent was removed and CH_2Cl_2 was added as the extracting solvent. The extracts were dried

Table 1
IR data, isolated yield and elemental analyses of Hpz^R (R = hp, op, dp) (**1–3**)

	IR [a] (cm^{-1})		Yield (%)	Molecular formula	Calculated (%)			Found (%)		
	ν(NH)	ν(CN)			C	H	N	C	H	N
1	3142	1615	53	$C_{15}H_{20}N_2O$	73.8	8.2	11.5	73.5	8.2	11.5
2	3142	1615	30	$C_{17}H_{24}N_2O$	75.0	8.8	10.3	74.6	8.8	10.1
3	3143	1614	50	$C_{19}H_{28}N_2O$	76.0	9.3	9.3	75.5	9.5	9.2

[a] In KBr discs.

Table 2
IR data, colour, isolated yield and elemental analyses of [Rh(Cl)(LL)(Hpz^R)] (LL = NBD, COD, 2CO; R = hp, op, dp) (**4**–**12**)

	IR [a] (cm^{-1})			Colour	Yield (%)	Molecular formula	Calculated (%)			Found (%)		
	ν(NH)	ν(CN)	ν(CO)				C	H	N	C	H	N
4	3291	1613		Yellow	60	$C_{22}H_{28}N_2OClRh$	55.6	5.9	5.9	55.3	5.9	5.9
5	3293	1613		Yellow	82	$C_{24}H_{32}N_2OClRh$	57.3	6.4	5.6	57.3	6.5	5.7
6	3297	1613		Yellow	75	$C_{26}H_{36}N_2OClRh$	58.8	6.8	5.3	58.6	6.7	5.3
7	3221	1614		Yellow	63	$C_{23}H_{32}N_2OClRh$	56.3	6.5	5.7	56.5	6.5	5.8
8	3227	1614		Yellow	55	$C_{25}H_{36}N_2OClRh$	57.9	6.9	5.4	57.5	6.8	5.5
9	3227	1615		Yellow	67	$C_{27}H_{40}N_2OClRh$	59.3	7.3	5.1	59.5	7.5	5.2
10	3326	1615	2086 2061 2015 1995	Red	60	$C_{17}H_{20}N_2O_3ClRh$	46.5	4.6	6.4	46.9	4.6	6.5
11	3327	1615	2087 2060 2014 1995	Red	73	$C_{19}H_{24}N_2O_3ClRh$	48.9	5.2	6.0	48.9	5.2	6.0
12-red	3329	1615	2086 2060 2014 1995	Red	19	$C_{21}H_{28}N_2O_3ClRh$	51.0	5.7	5.7	51.6	5.8	5.7
12-yellow	3285	1611	2069 2007	Yellow	68	$C_{21}H_{28}N_2O_3ClRh$	51.0	5.7	5.7	50.1	5.5	5.6

[a] In KBr discs.

on Na_2SO_4 and filtered. The solution was concentrated and a solid was obtained by precipitation with hexane. Yields are given in Table 1.

*2.2.2. Preparation of [Rh(Cl)(LL)(Hpz^R)] (LL = NBD, COD; R = hp, op, dp) (**4**–**9**)*

To a solution of [Rh(μ-Cl)(LL)]$_2$ (0.10 mmol) in CH_2Cl_2 (5 ml) was added the corresponding pyrazole Hpz^R (0.20 mmol). The reaction mixture was stirred for 1–2 h, and then the volume was reduced in vacuo to approximately 2 ml. Addition of hexane led to the precipitation of a yellow solid, which was filtered off, washed with hexane and dried in vacuo. Yields are given in Table 2.

*2.2.3. Preparation of [Rh(Cl)(CO)$_2$(Hpz^R)] (R = hp, op, dp) (**10**–**12**)*

To a solution of [Rh(μ-Cl)(CO$_2$)]$_2$ (0.15 mmol) in CH_2Cl_2 (2 ml) was added another of the corresponding pyrazole Hpz^R (0.30 mmol) in the same solvent (6 ml). The yellow solution was stirred for 2 h, and then the volume was reduced in vacuo to approximately 2 ml. Addition of hexane led to the precipitation of a yellow or a red solid depending on the pyrazole. The solid was filtered off, washed with hexane and dried in vacuo. Yields are given in Table 2.

2.3. X-ray structure determination

Red prismatic crystals of [Rh(Cl)(CO)$_2$(Hpz^{hp})] (**10**), [Rh(Cl)(CO)$_2$(Hpz^{op})] (**11**) and [Rh(Cl)(CO)$_2$(Hpz^{dp})] (**12**-red) and yellow crystals of [Rh(Cl)(CO)$_2$(Hpz^{dp})] (**12**-yellow) were grown by layering CH_2Cl_2 solutions with hexane. The crystals were mounted on a SMART CCD-Bruker diffractometer with graphite monochromated Mo–K$_\alpha$ radiation ($\lambda = 0.71073$ Å) operating at 50 kV and 20–25 mA. A summary of the fundamental crystal and refinement data for the four structures is given in Table 3.

For **12**-red a total of 5476 reflections were collected over a quadrant of the reciprocal space by combination of the two frame sets, and for **12**-yellow a total of 7316 reflections were collected over an hemisphere of the reciprocal space by combination of the three frame sets. Each exposure of 30 s covered 0.3° in ω. The first 50 frames were recollected at the end of the data collection to monitor crystal decay, and no appreciable decay was observed. The structure was solved by Patterson and Fourier techniques and refined by full-matrix least-squares on F^2 [23]. Anisotropic parameters were used in the last cycles of refinement for all non-hydrogen atoms, except the terminal carbon atoms C20 and C21 in **12**-red for which only two cycles of refinement were used and the thermal anisotropical factors fixed. The hydrogen atoms were included in calculated positions and refined as riding on the respective carbon atom with a common anisotropic displacement, except the hydrogen atom H2 bonded to N2 which was located in a Fourier synthesis, included and refined as riding on the N2 atom or fixed for **12**-red and **12**-yellow, respectively. Similar refinement to that of **12**-red has been carried out for **10** and **11**.

The largest residual peaks in the final difference map were 0.33, 0.24, 0.40 and 0.34 e $Å^{-3}$ for **10**, **11**, **12**-red and **12**-yellow, respectively, in the vicinity of the Rh atom. The refinement converged to R values of 0.031, 0.029, 0.042 and 0.035 for **10**, **11**, **12**-red and **12**-yellow, respectively.

3. Results and discussion

3.1. Synthetic and characterisation studies

3.1.1. Ligands Hpz^R ($R = hp$, op, dp) (**1**–**3**)

Compounds **1**–**3** were prepared by analogous procedures to those described for other pyrazol ligands [19,24–26]. The physical properties, IR data and elemental analyses are given in Table 1. The ^{1}H- and ^{13}C-NMR data are summarised in Tables 4 and 5, respectively. Assignment of the signals was made following the literature precedents [19,27–29].

In agreement with the related aryl-substituted pyrazoles, two tautomeric forms, Hpz^{3R} or Hpz^{5R}, or a tautomeric equilibrium could be expected for these heterocycles [27]. However, the NMR spectra of **1**–**3** show two well-defined signals as doublets for the H4 and H5 protons, indicating the presence of only one tautomer or a very fast equilibrium between the two tautomeric forms on the NMR time-scale at room temperature. On the other hand, the X-ray structure of the related pyrazole bearing the 4-phenoxyphenyl substituent demonstrated that this heterocycle was isolated as the 3-tautomer [19]. On this basis, we can suggest for the new pyrazoles **1**–**3** that the 3-tautomer must be present in both the solution and solid states.

3.1.2. Compounds $[Rh(Cl)(LL)(Hpz^R)]$ ($LL = NBD$, COD; $R = hp$, op, dp) (**4**–**9**)

Reactions of the dimers $[Rh(\mu\text{-}Cl)(LL)]_2$ (LL = NBD, COD) with Hpz^R (R = hp, op, dp) were performed in dichloromethane in 1:2 molar ratios (Scheme 2). All the

Table 3
Crystal and refinement data for $[Rh(Cl)(CO)_2(Hpz^R)]$ (R = hp, op, dp) (**10**, **11**, **12**-red, **12**-yellow)

	10	**11**	**12**-red	**12**-yellow
Empirical formula	$C_{17}H_{20}ClN_2O_3Rh$	$C_{19}H_{24}ClN_2O_3Rh$	$C_{21}H_{28}ClN_2O_3Rh$	$C_{21}H_{28}ClN_2O_3Rh$
Formula weight	438.71	466.76	494.81	494.81
Temperature (K)	296(2)	296(2)	296(2)	296(2)
Crystal system	Monoclinic	Monoclinic	Monoclinic	Triclinic
Space group	$P2_1/c$	$P2_1/c$	$P2_1/c$	$P\bar{1}$
Unit cell dimensions				
a (Å)	19.357(2)	21.315(2)	23.099(3)	7.6304(8)
b (Å)	13.930(2)	13.982(1)	14.021(2)	10.019(1)
c (Å)	7.092(1)	7.070(1)	7.059(1)	15.738(2)
α (°)				82.273(2)
β (°)	97.826(3)	97.721(2)	93.168(3)	84.567(2)
γ (°)				71.782(2)
V (Å^3)	1894.6(4)	2088.0(3)	2282.7(6)	1130.7(2)
Z	4	4	4	2
$\rho_{calc.}$ (g cm^{-3})	1.538	1.485	1.440	1.453
μ (mm^{-1})	1.058	0.965	0.887	0.896
$F(000)$	888	952	1016	508
Crystal size (mm)	$0.28 \times 0.12 \times 0.06$	$0.26 \times 0.08 \times 0.08$	$0.50 \times 0.08 \times 0.03$	$0.15 \times 0.10 \times 0.08$
Scan technique	ϕ and ω	ϕ and ω	ϕ and ω	ϕ and ω
Data collected	(−8, −13, −6) to (19, 13, 6)	(−23, −15, −7) to (23, 10, 7)	(−23, −14, −7) to (15, 14, 3)	(−9, −12, −22) to (10, 14, 19)
θ range (°)	1.81–20.81	1.75–23.25	1.70–21.96	3.41–30.56
Reflections collected	4008	9179	5476	7316
Independent reflections	1761 ($R_{int} = 0.07$)	2990 ($R_{int} = 0.05$)	2396 ($R_{int} = 0.08$)	5395 ($R_{int} = 0.05$)
Reflections observed [$I \geq 2\sigma(I)$]	1101	1778	1166	2566
R [a]	0.031	0.029	0.042	0.035
Rw_F [b]	0.063	0.066	0.080	0.070

[a] $\Sigma[|F_o| - |F_c|]/\Sigma|F_o|$.
[b] $(\Sigma[w(F_o^2 - F_c^2)^2]/\Sigma[w(F_o^2)^2])^{1/2}$.

Table 4
^{1}H-NMR data of the pyrazoles Hpz^R (R = hp, op. dp) (**1**–**3**) in $CDCl_3$ at 298 K

	Pyrazole			–C_6H_4–		–OR	
	NH	H4	H5	H*o*	H*m*		
1	n.o.	6.51d $J_{45} = 2.1$	7.58d	7.63d $J_{om} = 8.8$	6.92d	CH_2-1′: 3.97t CH_2-2′: 1.78q CH_2-3′,4′,5′: 1.5–1.1 m CH_3-6′: 0.89t	$J_{1'2'} = 6.5$ $J_{2'3'} = 7.8$ $J_{5'6'} = 6.8$
2	n.o.	6.52d $J_{45} = 2.1$	7.58d	7.63d $J_{om} = 8.6$	6.91d	CH_2-1′: 3.96t CH_2-2′: 1.78q CH_2-3′,4′,5′,6′,7′: 1.5–1.1 m CH_3-8′: 0.87t	$J_{1'2'} = 6.5$ $J_{2'3'} = 7.2$ $J_{7'8'} = 6.8$
3	n.o.	6.51d $J_{45} = 2.1$	7.58d	7.63d $J_{om} = 8.7$	6.92d	CH_2-1′: 3.96t CH_2-2′: 1.78q CH_2-3′,4′,5′,6′,7′,8′9′: 1.5–1.1 m CH_3-10′: 0.86t	$J_{1'2'} = 6.6$ $J_{2'3'} = 7.4$ $J_{9'10'} = 6.7$

n.o.: not observed.

Table 5
$^{13}C\{^1H\}$-NMR data of the pyrazoles Hpz^R (R = hp, op. dp) (**1**–**3**) in $CDCl_3$ at 298 K

	Pyrazole carbons			–C_6H_4–				–OR
	C3	C4	C5	Cα	C*o*	C*m*	C*p*	
1	148.4	102.0	133.7	124.0	127.0	114.8	159.2	C1′: 68.0 C2′,3′,4′,5′: 31.5, 29.1, 25.6, 22.5 C6′: 13.9
2	148.4	102.1	133.7	124.0	127.1	114.8	159.3	C1′: 68.1 C2′,3′,4′,5′,6′,7′: 31.8, 29.3, 29.2, 29.1, 26.0, 22.6 C8′: 14.0
3	148.4	102.1	133.7	124.0	127.1	114.8	159.3	C1′: 68.1 C2′,3′,4′,5′,6′,7′,8′,9′: 31.9, 29.6, 29.4, 29.3, 29.2, 26.0, 22.7 C10′: 14.1

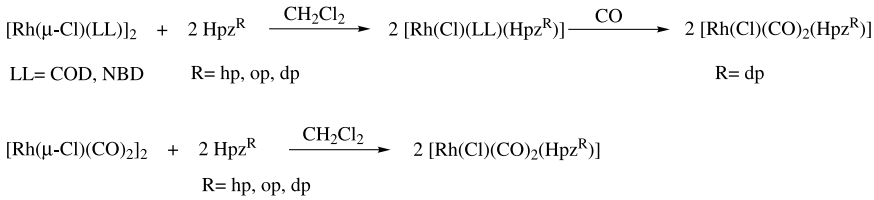

Scheme 2.

complexes isolated are yellow air-stable solids characterised as [Rh(Cl)(LL)(Hpz^R)] (LL = NBD, COD; R = hp, op, dp) (**4**–**9**) by analytical and spectroscopic (IR and ^{1}H-NMR) techniques (Tables 2 and 6). The ^{1}H-NMR spectra at room temperature consist of well-resolved signals corresponding to the coordinated pyrazol ligand with the expected intensity ratios and multiplicities. However, the olefinic protons appear as broad signals, which is attributed to the conformational fluxionality of the coordinated diene, as has been previously observed in related Rh(I) complexes [15,19,30].

*3.1.3. Compounds [Rh(Cl)(CO)$_2$(Hpz^R)] (R = hp, op, dp) (**10**–**12**)*

The complexes [Rh(Cl)$(CO)_2$(Hpz^R)] (R = hp, op, dp) (**10**–**12**) were formed in a single step by reaction of the dimer [Rh(μ-Cl)$(CO)_2]_2$ with the corresponding pyrazole Hpz^R in dichloromethane in 1:2 molar ratios (Scheme 2). An alternative synthesis previously used in related compounds [15,19] consisting of bubbling CO through a dichloromethane solution of [Rh(Cl)-(LL)(Hpz^R)] (LL = NBD, COD) also gave rise to the dicarbonyl complexes **10**–**12**, but only compound **12**,

pound **12**, having the 10-carbon chain substituent, was isolated pure in a good yield.

In all cases, the reaction solution was yellow but some differences were found for the isolated solid products. Compounds **10** and **11** were obtained by partial evaporation of the dichloromethane solution and precipitation with hexane as red microcrystalline solids, which after recrystallisation in dichloromethane–hexane gave red needle crystals. On the other hand, compound **12** precipitated as a yellow solid from the reaction solution, which was filtered off and characterised by analytical and spectroscopic data as the dicarbonyl derivative $[Rh(Cl)(CO)_2(Hpz^{dp})]$ (**12**-yellow). From the filtrate a second product was formed as red microcrystals by slow crystallisation at room temperature. The analytical and spectroscopic data showed that this red product corresponded to the same dicarbonyl complex $[Rh(Cl)(CO)_2(Hpz^{dp})]$ but in a different solid form (**12**-red). The analytical and spectroscopic (IR and ^{1}H-NMR) data of the dicarbonyl complexes **10**–**12** are collected in Tables 2 and 6.

The ^{1}H-NMR spectra of **10**–**12** in $CDCl_3$ solution at room temperature show all the expected signals. No differences between the spectra of the red and yellow forms for **12** were found, indicating that the difference between the forms applies only to the solid state. In all cases, the presence of a single tautomer with the corresponding pyrazole bearing the substituents at the 3 position, was deduced from the values of the coupling constant between the H4 and H5 protons of ca. 2 Hz (lower values of ca. 1.5 Hz are indicative of a substitution at the 5 position) [15,19,29,31–33]. Consequently no evidences of a metallotropic equilibrium were found.

In all spectra a signal at ca. 12 ppm was observed which corresponds to the NH proton. Also remarkable is the presence of triplets for the H4 and H5 protons of

Table 6
^{1}H-NMR data of compounds $[Rh(Cl)(LL)(Hpz^R)]$ (LL = NBD, COD, 2CO; R = hp, op, dp) (**4**–**12**) in $CDCl_3$ at 298 K

	Pyrazole			–C_6H_4–		–OR		LL
	NH	H4	H5	H*o*	H*m*			
4	12.07br	6.39d $J_{45}=2.1$	6.74d	7.41d $J_{om}=8.7$	6.91d	CH_2-1′: 3.96t CH_2-2′: 1.77q CH_2-3′,4′,5′: 1.5–1.2m CH_3-6′: 0.89t	$J_{1'2'}=6.5$	CH_2-7: 1.5–1.2 CH-2,3,5,6: 4.00br s CH-1,4: 3.85 br s
5	12.07br	6.37d $J_{45}=2.1$	6.73d	7.40d $J_{om}=8.7$	6.90d	CH_2-1′: 3.95t CH_2-2′: 1.75q CH_2-3′,4′,5′,6′,7′: 1.6–1.2m CH_3-8′: 0.86t	$J_{1'2'}=6.6$ $J_{7'8'}=6.9$	CH_2-7: 1.6–1.2 CH-2,3,5,6: 4.04br s CH-1,4: 3.84br s
6	12.08br	6.34 br	6.72br	7.40d $J_{om}=8.7$	6.90d	CH_2-1′: 3.95t CH_2-2′: 1.76q CH_2-3′,4′,5′,6′,7′,8′,9′: 1.5–1.2m CH_3-10′: 0.86t	$J_{1'2'}=6.6$ $J_{9'10'}=6.9$	CH_2-7: 1.5–1.2 CH-2,3,5,6: 4.04br s CH-1,4: 3.84br s
7	12.50br	6.42d $J_{45}=2.1$	7.04d	7.43d $J_{om}=8.7$	6.91d	CH_2-1′: 3.95t CH_2-2′: 1.84m CH_2-3′,4′,5′: 1.5–1.2m CH_3-6′: 0.86t	$J_{1'2'}=6.6$ $J_{5'6'}=6.8$	CH-1,2,5,6: 4.40br s CH_2-3,4,7,8: 2.45m, 1.84m
8	12.50br	6.44br	7.06br	7.45d $J_{om}=8.7$	6.93d	CH_2-1′: 3.97t CH_2-2′: 1.76q CH_2-3′,4′,5′,6′,7′: 1.5–1.2m CH_3-8′: 0.88t	$J_{1'2'}=6.6$ $J_{7'8'}=6.6$	CH-1,2,5,6: 4.22br s CH_2-3,4,7,8: 2.49m, 1.85m
9	12.49br	6.42d $J_{45}=2.1$	7.04d	7.43d $J_{om}=8.7$	6.91d	CH_2-1′: 3.95t CH_2-2′: 1.77q CH_2-3′,4′,5′,6′,7′,8′,9′: 1.5–1.1m CH_3-10′: 0.86t	$J_{1'2'}=6.6$ $J_{9'10'}=6.9$	CH-1,2,5,6: 4.37br s CH_2-3,4,7,8: 2.46m, 1.85m
10	12.18br	6.55t $J_{45}=2.1$ $J_{NH4}=2.1$	7.59t	7.46d $J_{om}=8.7$	6.95d	CH_2-1′: 3.98t CH_2-2′: 1.78q CH_2-3′,4′,5′: 1.5–1.3m CH_3-6′: 0.90t	$J_{1'2'}=6.6$ $J_{5'6'}=6.9$	
11	12.18br	6.55t $J_{45}=2.1$ $J_{NH4}=2.1$	7.59t	7.46d $J_{om}=9.0$	6.95d	CH_2-1′: 3.97t CH_2-2′: 1.78q CH_2-3′,4′,5′,6′,7′: 1.5–1.2m CH_3-8′: 0.90t	$J_{1'2'}=6.6$ $J_{7'8'}=6.9$	
12	12.18br	6.55t $J_{45}=2.1$ $J_{NH4}=2.1$	7.59t	7.46d $J_{om}=8.7$	6.95d	CH_2-1′: 3.97t CH_2-2′: 1.78q CH_2-3′,4′,5′,6′,7′,8′,9′: 1.5–1.2m CH_3-10′: 0.86t	$J_{1'2'}=6.6$ $J_{9'10'}=6.9$	

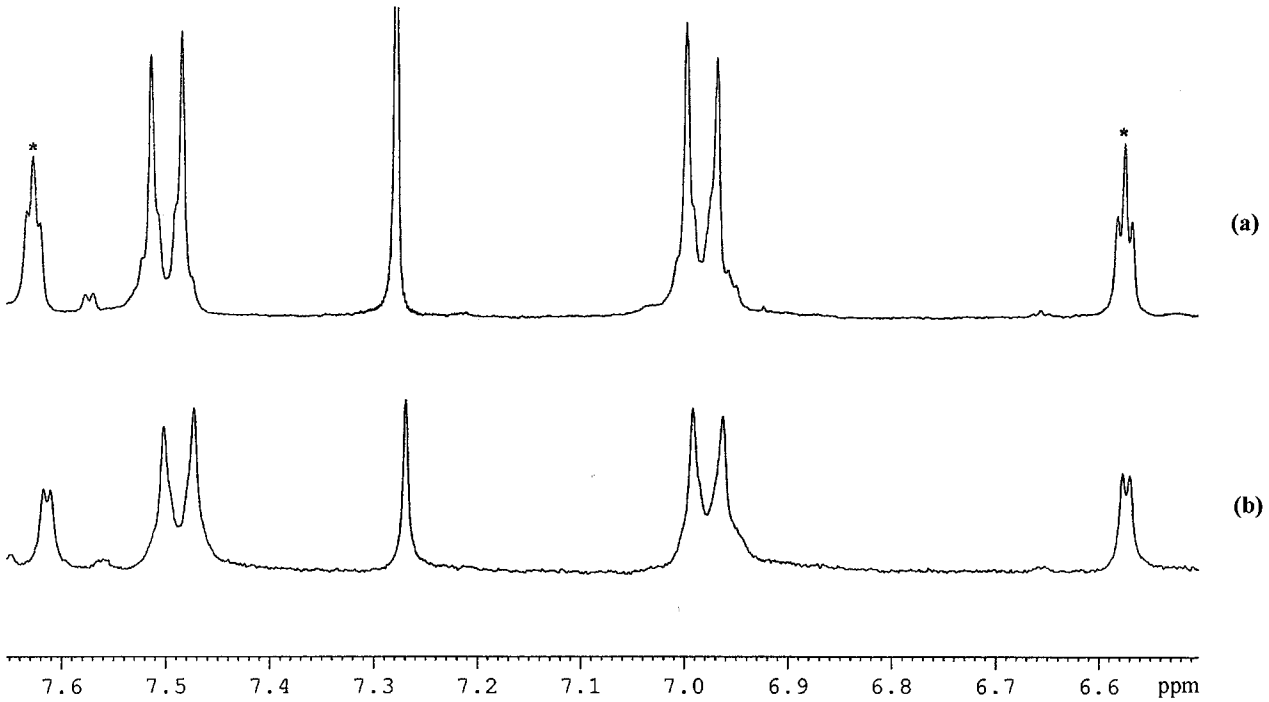

Fig. 2. ^{1}H-NMR spectra in the aromatic region for **12** (a) and after irradiation on the NH signal (b). The asterisks show the H4 and H5 protons of the pyrazole.

the pyrazole, which is attributed to an unusual coupling between these protons with the NH proton, as confirmed from the spectra obtained by irradiation on the NH signal (Fig. 2).

The IR spectra of **10**–**12** have been studied both in the solid state and in solution. In dichloromethane all three compounds showed the two expected ν(CO) bands at ca. 2088 and 2016 cm^{-1}, consistent with a mononuclear *cis*-dicarbonyl complex. However, in the solid state four bands at ca. 2086, 2060, 2015 and 1995 cm^{-1} were observed for **10**, **11** and **12**-red. By contrast only two bands at 2069 and 2007 cm^{-1} were found for **12**-yellow. The red colour and the extra bands are not typical of mononuclear square-planar Rh(I) complexes and therefore these results are probably a consequence of their particular stacking, possibly analogous to that observed in related complexes which display one-dimensional metal–metal interactions [15,16,34]. The yellow form probably corresponds to a different packing arrangement in which metal–metal interactions for chains of complexes are not present.

The electronic spectra in the dichloromethane solution of both the yellow and red forms of **12** were identical, consistent with the presence of only one form in solution. The pattern of bands, which was also found for the red forms of **10** and **11**, consists of a main band centred at ca. 310 nm similar to that observed in their corresponding ligands ($\sim$320 nm) assigned to a $\pi \rightarrow \pi^*$ intraligand transition [14]. A second absorption as a shoulder at ca. 340 nm ($\varepsilon = 4600$ dm^3 mol^{-1} cm^{-1}) could be associated with a transition involving metal orbitals.

The above results indicate that two polymorphs (red and yellow) were isolated for **12**, whilst only one (red form) for the related **10** and **11**. Then the length of the alkyloxy substituent on the pyrazol ligands appears to be responsible for the differences observed in polymorphic behaviour.

The existence of polymorphic forms for related mesomorphic compounds has previously been reported. In a recent work, Bruce et al. described two modifications (one burgundy and other orange) of the complex *cis*-[Ir(Cl)(CO)$_2$(9-OPhVPy)] (9-OPhVPy = *trans*-4-nonyloxy-4′stilbazole), although no X-ray crystalline structures of any of those forms were reported [10]. However, their IR patterns in the carbonyl region were analogous to those described above for our red and yellow materials. Also two polymorphic forms (yellow and red or yellow and blue) were found, respectively, for [Rh(CO)$_2$(β-diketonate)] (β-diketonate = 3-[(4′-((4″-*n*-decyloxybenzoyl)oxy)phenoxy)carbonyl]-2,4-pentanedionate) and [Ir(CO)$_2$(β-diketonate)] (β-diketonate = 3-[(4′-((4″-*n*-decyloxybenzoyl)oxy)phenoxy)carbonyl]-2,4-pentanedionate, 3-[(4′-(4″-*n*-decyloxybenzoyl)oxy)-benzyl]-2,4-pentanedionate) [14]. In this case, the X-ray crystal structure of the yellow form of [Ir(CO)$_2$(β-diketonate)] (β-diketonate = 3-[(4′-((4″-*n*-decyloxybenzoyl)-oxy)phenoxy)carbonyl]-2,4-pentanedionate) indicated

molecular stacking along the *b*-axis with the metal coordination planes being parallel but in a disposition which appeared to exclude direct metal–metal interactions [14].

In contrast to the above examples, no polymorphic forms have previously been described for complexes of the type $[Rh(Cl)(CO)_2(Hpz^R)]$. Indeed a red or blue compound has exclusively been found for these complexes containing unsubstituted or some 3(5) or 3 and 5 substituted pyrazol ligands [15,16,19], and in addition the complex $[Rh(Cl)(CO)_2(Hpz^{Me2,4R})]$ ($Hpz^{Me2,4R}$ = 4-[(4′-((4″-*n*-decyloxybenzoyl)oxy)phenoxy)carbonyl]-3,5-dimethylpyrazole) containing 4-substituted pyrazole has recently been isolated as a yellow solid [14].

With the above precedents in mind, we were interested in proving why increase of the length of the substituents at the 3 position on the pyrazole is responsible for the polymorphism for **12**. Crystals of sufficient quality for X-ray diffraction of the two polymorphs were isolated after repeated recrystallisations and their X-ray structures solved. We have similarly solved the X-ray crystal structures of the red compounds **10** and **11** in order to deduce the influence of the length of the chains.

3.2. X-ray crystal structures of **10**–**12**

The molecular geometry of the red form of $[Rh(Cl)(CO)_2(Hpz^{dp})]$ (**12**-red) is shown in Fig. 3, and Table 7 lists the selected bond distances and angles. A square-planar environment around the Rh atom is defined by the Cl ligand, two CO groups and the pyrazolic N atom, the Rh atom being displaced by 0.0011 Å from the best least-squares plane N1C1C2Cl1. The pyrazol ring is rotated 16.1(3)° from the coordination plane and the phenyl ring deviates by 12.5(3) and 12.4(2)° from the pyrazol plane and the coordination plane, respectively. However, the best least-squares plane defined for the carbon atoms C12–C21 of the aliphatic chain presents a higher deviation from the above-mentioned planes, the angle with the phenyl ring being 62.6(3)° (Table 8). An interesting feature is the hydrogen bonding interaction between the NH group and the Cl ligand with a N2···Cl1 distance of 3.105(7) Å (Table 9).

However, the most interesting aspect of the structure is the molecular packing which consists of stacking of the square-planar unities along the crystallographic *c*-axis to form one-dimensional chains which are almost

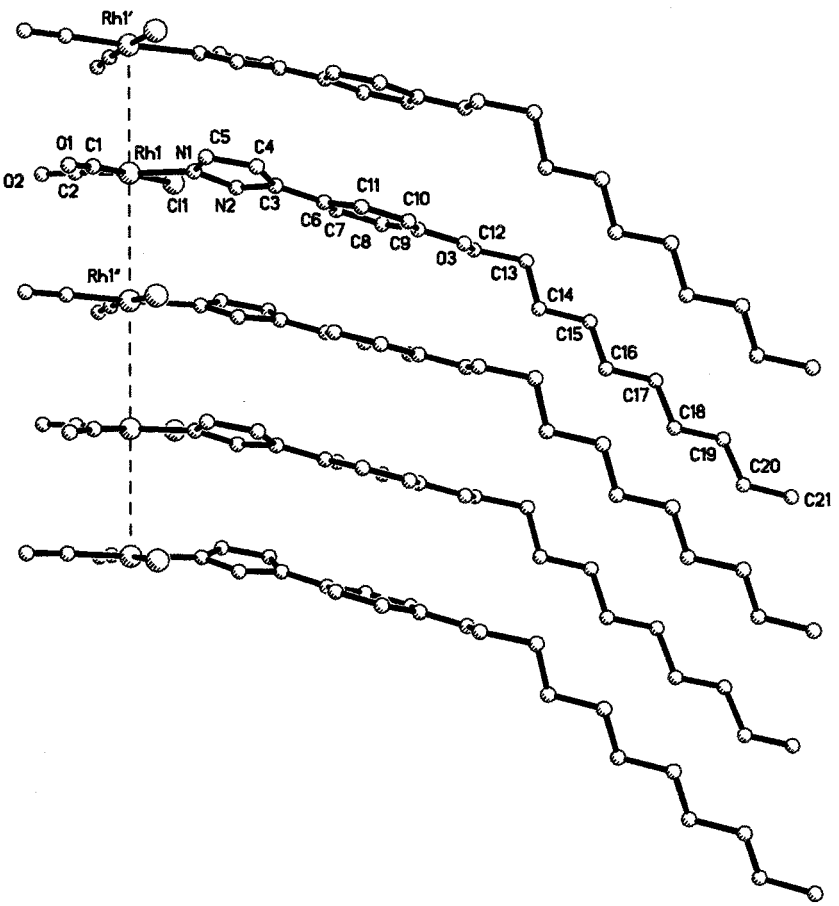

Fig. 3. Stacking along the *c*-axis of **12**-red showing the atomic numbering scheme. Hydrogen atoms have been omitted for clarity. Compounds **10** and **11** present the same disposition.

Table 7
Selected bond distances (Å) and bond angles (°) for [Rh(Cl)(CO)$_2$(Hpz^{dp})] (**12**-red and **12**-yellow)

	12-red	**12**-yellow
Rh–N1	2.061(7)	2.081(3)
Rh–C1	1.829(8)	1.845(4)
Rh–C2	1.803(9)	1.835(4)
Rh–Cl1	2.361(2)	2.338(1)
C1–O1	1.135(8)	1.126(4)
C2–O2	1.165(9)	1.137(4)
N1–N2	1.321(7)	1.355(3)
N1–C5	1.365(9)	1.327(4)
N2–C3	1.341(8)	1.334(4)
N2–H2	0.821	0.971
N1–Rh–C1	90.3(3)	90.7(1)
N1–Rh–C2	178.1(4)	176.9(1)
N1–Rh–Cl1	89.4(2)	88.7(1)
C1–Rh–C2	90.8(4)	89.6(2)
C1–Rh–Cl1	178.4(3)	177.7(1)
C2–Rh–Cl1	89.5(3)	90.9(1)
H2–N2–N1	121.1	117.7
H2–N2–C3	122.7	128.4

Table 8
Selected angles (°) between the least-squares sets defined by the specified atoms for [Rh(Cl)(CO)$_2$(Hpz^{dp})] (**12**-red and **12**-yellow)

		12-red	**12**-yellow
1 — C1N1C2Cl1	1–2	16.1(3)	12.0(1)
2 — N1N2C3C4C5	1–3	12.4(3)	34.1(1)
3 — C6C7C8C9C10C11	1–4	64.3(2)	37.5(2)
4 — C12C13C14C15C16C17C18-C19C20C21	2–3	12.5(3)	23.3(1)
	2–4	75.1(3)	26.9(2)
	3–4	62.6(3)	3.6(2)

Table 9
Interaction distances (Å) and angles (°) for [Rh(Cl)(CO)$_2$(Hpz^{dp})] (**12**-red and **12**-yellow)

	12-red	**12**-yellow
N2–H2	0.821	0.971
N2···Cl1	3.105(7)	3.059(3)
Cl1···H2	2.582	2.384
Rh···Cl1′		3.921(1)
N2–H2···Cl1′	123.0	126.2

(′) Symmetry operation: $1-x$, $2-y$, $1-z$.

linear (178.86(5)°). The coordination planes are almost orthogonal to the *b*-axis, and the Rh–Rh distance of 3.5296(5) Å is short enough to be considered a metal–metal interaction along the stacking axis.

The columnar arrangement (Fig. 3) implicates an alternatively staggered disposition of coordinated groups around the metal, so that all the pyrazol planes are alternatively staggered as well as those of the phenyl rings and consequently the alkyl chains, in order to minimise steric congestion. As a consequence of the parallel disposition of the molecular cores, defined by the coordination, pyrazol and phenyl planes, in each column a close approach between the Rh centres along the stacking axis should be favoured. However, this effect could partially be inhibited by the molecular bending produced by the long-chain substituent.

Adjacent molecules in the *ab* plane are arranged head-to-tail along the *b*-axis and in the same sense through the molecular axis (Fig. 4). Individual stacks are spaced at distances greater than 5 Å from one another giving rise to Rh···Rh distances longer than 10 Å.

Overall the structure can therefore be described as formed by layers in the *ac* plane with some interdigitation between the consecutive layers.

The structure of **12**-red shows that one-dimensional metal–metal interactions exist in the solid state despite the steric consequences of the alkyl long-chains give rise to an intermolecular Rh···Rh distance 0.13 Å longer than that observed in the related complex [Rh(Cl)(CO)$_2$(Hpz^{An})] for which the same type of molecular stacking had been found [15]. However, the columnar chain structure, which is very scarce amongst rhodium derivatives, is maintained.

Complexes **10** and **11** are almost isostructural with the above-described **12**-red. The slight differences observed in the Rh···Rh distances and Rh···Rh···Rh angles (Table 10) suggest that the increase in the length of the alkyl chain favours the intermetallic interaction.

The crystal structure of the yellow form of [Rh(Cl)(CO)$_2$(Hpz^{dp})] (**12**-yellow) was solved and compared with that of **12**-red. Selected bond distances and angles are recovered in Table 7. Comparing both structures, firstly there are some differences between the

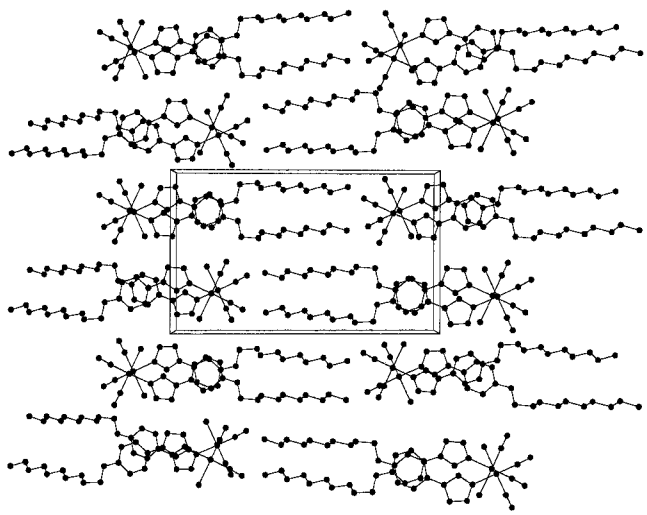

Fig. 4. Drawing of the packing in **12**-red in the *ab* plane.

Table 10
Rh···Rh′ distances (Å) and Rh′···Rh···Rh″ angles (°) along the columnar stacking for complexes [Rh(Cl)(CO)$_2$(Hpz^R)] (R = hp, op, dp) (**10**–**12**)

	Rh···Rh′	Rh′···Rh···Rh″
10 [a]	3.5464(5)	178.88(4)
11 [a]	3.5354(4)	178.82(2)
12-red [a]	3.5296(5)	178.86(5)
12-yellow [b]	3.3631(1)	

[a] Symmetry operation: (′) x, $1/2-y$, $1/2+z$; (″) x, $1/2-y$, $-1/2+z$.
[b] Symmetry operation: (′) $1-x$, $2-y$, $1-z$.

geometrical parameters of the molecules of each form. In particular, the molecular geometry of **12**-yellow, as shown in Fig. 5, is apparently closer to planarity as defined by angles between the coordination plane and those of the pyrazol ring, the aromatic group and the best least-squares plane of the chain atoms (Table 8).

In striking contrast, the molecular packing in crystals of **12**-yellow is dominated by the stacking of dimeric units along the *a*-axis. Each almost planar molecule in columnar stacking of square metal-centred units interacts with a second molecule of the neighbour column via their corresponding Cl ligands. Specifically, Cl of one coordination plane lies above that of the related molecule and at the same time Cl of the latter is situated below the rhodium-centred coordination plane of the first one (Figs. 5 and 6). Both Rh–Cl distances of 3.921(1) Å suggest the presence of weak intermolecular interactions through Cl bridges and as a consequence the Rh···Rh distance between the metal centres of interacting molecules is 3.3631(1) Å. Therefore, the structure could be described as formed of weakly bonded dimers. These dimers are stacked along the *a*-axis in a linear fashion but the Rh···Rh distance between dimers along this axis is too long (7.6304(8) Å) for metal–metal interactions.

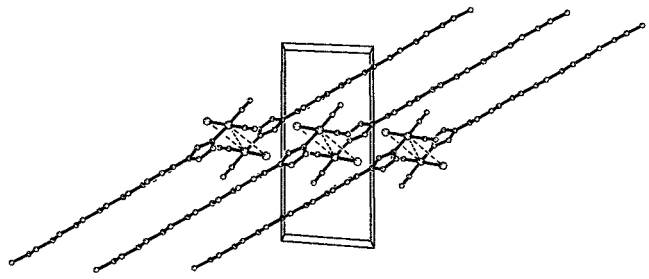

Fig. 6. Drawing of the packing through the *b*-axis in **12**-yellow showing the rod-like distribution.

It is reasonable to ask why the structure of the yellow form consists of dimers stacked rather than the uniform stacking arrangement of monomers observed in the red form. By the inspection of the nearest contacts inside the structure we observed that a hydrogen bonding interaction exists between the N–H hydrogens and the Cl atoms which was stronger than that found in the red form (**12**-red) described above (Table 9). This enhancement could be a consequence of the orientation of the Cl ligand to act as a bridge in the dimer. In other words the Cl ligand of each molecule engages in both *intra*- and *inter*-molecular interactions with an intramolecular NH group and the Rh atom of the neighbour, H2···Cl1···Rh1′ (Fig. 5). This feature is also supported by the IR results of the N–H frequency values: the yellow form presents a lowering of ca. 60 cm^{-1} compared to the red one (Table 2) as a consequence of the weakness of N–H bond produced by the hydrogen bonding interaction.

The above structural results together with the fact that the yellow form is favoured with long-chain substituents need further comments. An explanation

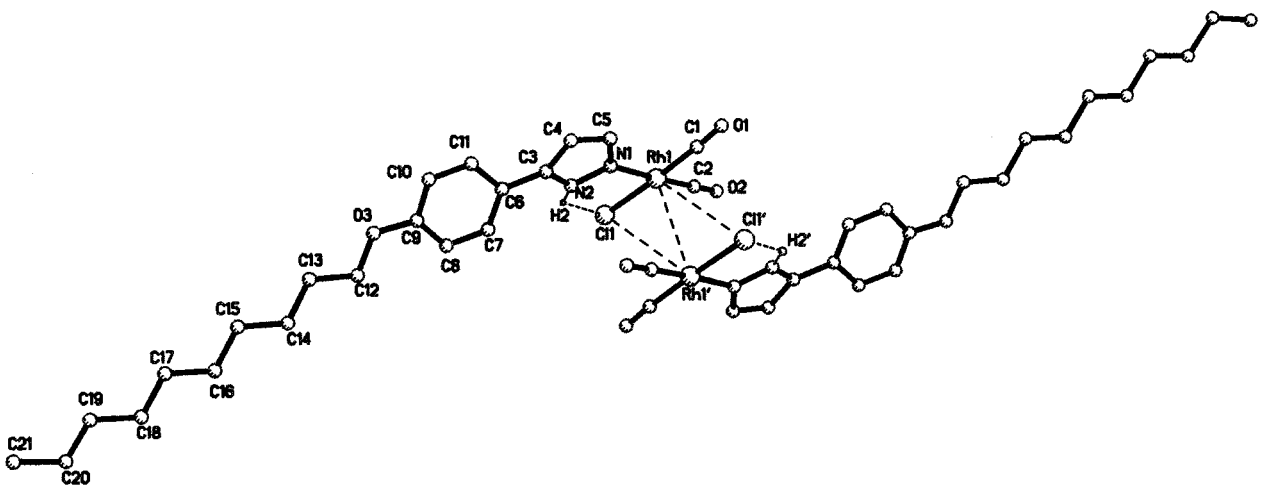

Fig. 5. Dimeric unity in **12**-yellow showing the atomic numbering scheme. Hydrogen atoms, except H2, have been omitted for clarity.

emerges by considering the interdigitated layer structure of the red forms in which some gliding between layers in order to obtain a higher proximity between metal centres of molecules of adjacent columns would be easier in **12** than in **10** and **11** (Fig. 1). In this way, the dimeric unities of the yellow form are raised only for **12** at room temperature. Consistent with this proposal the red form is converted to the yellow one by heating as observed by polarised optical microscopy.

Table 11
Phase properties of compounds **1**–**12** determined by DSC

	Transition	T (°C)	ΔH (kJ mol^{-1})
1	$K \rightarrow IL$	59	13.5
2	$K \rightarrow IL$	67	21.8
3	$K \rightarrow IL$	77	32.8
4	$K \rightarrow IL$	105	19.2
5	$K \rightarrow IL$	119	26.2
6	$K \rightarrow IL$	115	17.3
7	$K \rightarrow IL$	107	22.9
8	$K \rightarrow IL$	98	22.1
9	$K \rightarrow IL$	101	23.3
10	$K_1 \rightarrow K_1'$	88 [a]	9.5
	$K_1 \rightarrow IL$		
	$K_2 \rightarrow IL$	103	19.7
11	$K_1 \rightarrow K_1'$	73	11.9
	$K_1 \rightarrow IL$	91 [b]	[b]
	$K_2 \rightarrow IL$	99	21.6
12-red	$K_1 \rightarrow K_1'$	68	11.2
	$K_1 \rightarrow IL$	95 [c]	31.5
	$K_2 \rightarrow IL$		
12-yellow	$K_2 \rightarrow IL$	98	46.0

[a] The transformations $K_1 \rightarrow K_1'$ and $K_1 \rightarrow IL$ appear overlapped.
[b] This transition is observed as a weak and broad signal (ΔH value has not been possible to be determined).
[c] The two melting processes $K_1 \rightarrow IL$ and $K_2 \rightarrow IL$ appear overlapped.

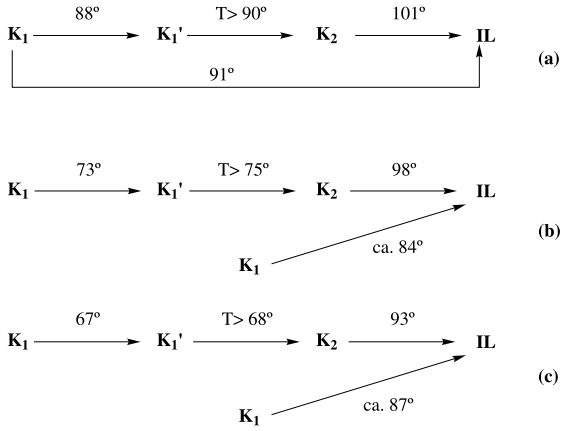

Scheme 3. Phase transitions observed by polarised microscopy for the red compounds [Rh(Cl)(CO)$_2$(Hpz^R)]: (a) R = hp **10**; (b) R = op **11**; (c) R = dp **12**-red.

3.3. Thermal studies

The thermal behaviour of the pyrazol ligands **1**–**3** and their corresponding Rh–dicarbonyl complexes **10**–**12** were studied by polarised optical microscopy and differential scanning calorimetry. The results are recovered in Table 11. The thermal data from the olefinic derivatives **4**–**9** are also included.

Unfortunately no mesomorphism was observed for any compound. However, thermochromic behaviour was found for the dicarbonyl complexes **10**–**12**. Specifically, on heating the corresponding microcrystalline red forms a transformation to a yellow solid phase occurred in all cases. This transition from the red to yellow solid is a slow process which occurs over a wide temperature range. In all cases, before the yellow solid begins to form, a darkening is observed.

The evolution from the red to the yellow phase is slower and has a higher onset temperature for **11** than for **12**-red, these observations being consistent with the greater ease of gliding between layers in **12**-red in relation to another which has shorter chains. Compound **10** follows the same sequence of temperature for that transformation. However, in this case it is difficult to observe the evolution to the yellow phase because this process is overlapped with the melting of the red solid. Melting of some of the red solid was also observed for **11** and **12**-red at temperatures of ca. 85 and 87 °C. Finally, for the three compounds melting of the yellow solid phase is clearly observed at similar temperatures (ca. 95 °C).

The sequence of phase changes of these compounds is shown in Scheme 3, and that for **12**-red is taken as a representative example:

- The sample exists as red needle-like crystals (K_1) at room temperature.
- When the sample is heated to 67 °C a darkening of the solid occurs (K_1').
- By heating to 69 °C the yellow solid phase (K_2) begins to formed.
- By holding the temperature of the sample at 87 °C for 20 min, the red crystalline form (K_1) melts.
- Finally, by heating to 95 °C the yellow form (K_2) melts.

This double melting behaviour observed by polarising microscopy is also confirmed by DSC measurements. The precise temperature of the red–yellow phase transition could not be determined by DSC observations because this phase transition is very slow and because the superheating of K_1 crystals occurs easily. Although the superheating of K_1 crystals originates such double melting behaviour, at the same time this makes it difficult to detect the precise temperature of the solid–solid phase transition.

For compound **12**-yellow only the expected transition to isotropic liquid is observed at 97 °C by both DSC and polarising microscope.

The double melting behaviour and the textures observed by polarising microscopy could suggest for these compounds [Rh(Cl)(CO)$_2$(Hpz^R)] (R = hp, op, dp) a thermal behaviour close to mesomorphism. Such multiple melting behaviour has been related to phenomena for states between crystals and liquid crystals [35].

On the other hand, in all cases, on cooling the isotropic liquid at 10 °C per minute, the thermograms show two broad peaks corresponding to transformations to crystalline phases at ca. 65–90 °C, in agreement with that observed by polarising light microscope.

By comparing the thermal behaviour of the complexes **10**–**12** with that of their respective ligands **1**–**3**, an increase in the melting points is observed. All the types of interactions found in the described complexes appear to be responsible for this increase.

4. Concluding remarks

Two polymorphs (yellow and red) have been isolated for [Rh(Cl)(CO)$_2$(Hpz^{dp})] (**12**) in contrast to the single red one found for compounds [Rh(Cl)(CO)$_2$(Hpz^R)] (R = hp, op; **10** and **11**). The compounds **10**, **11** and **12**-red are isostructural, their structures being defined by a one-dimensional stacking of planar molecules with considerable metal–metal interactions along the *c*-axis. The yellow form (**12**-yellow) is dominated by interactions of the types NH···Cl and Rh–Cl···Rh, and therefore, as a consequence, dimeric unities occur. These dimers are stacked through the *a*-axis but the large Rh···Rh distance along this axis precludes an intermolecular interaction. Transformation of the red form to the yellow one could be easily understood as a consequence of gliding of layers until intermolecular Rh···Cl and Rh···Rh interactions in the dimeric unit prevail over the Rh···Rh ones inside the one-dimensional stacking.

No liquid crystal properties have been found for the complexes. However, a concise examination of the molecular structure of **12**-yellow, as depicted in Fig. 6, suggests an interesting rod-like molecular form of the dimers. Further effort will be made to prepare molecular dimers with the above characteristics.

5. Supplementary material

Crystallographic data for the structural analysis have been deposited with the Cambridge Crystallographic Data Centre, CCDC nos. 161484–161487 for **10**, **11**, **12**-red and **12**-yellow, respectively. Copies of this information may be obtained free of charge from The Director, CCDC, 12 Union Road, Cambridge CB2 1EZ, UK (Fax: +44-1223-336033; e-mail: deposit@ccdc.cam.ac.uk or www: http://www.ccdc.cam.ac.uk).

Acknowledgements

Financial support from the DGES of Spain is gratefully acknowledged (Project no. PB98-0766).

References

[1] B. Donnio, D.W. Bruce, Struct. Bond. 95 (1999) 193.
[2] S.R. Collinson, D.W. Bruce, in: J.P. Sauvage (Ed.), Transition Metals in Supramolecular Chemistry, Wiley, Chichester, 1999, pp. 285–369 (chap. 7).
[3] J.L. Serrano (Ed.), Metallomesogens. Synthesis, Properties and Applications, VCH, New York, 1996.
[4] A. Hudson, P.M. Maitlis, Chem. Rev. 93 (1993) 861.
[5] P. Espinet, M.A. Esteruelas, L.A. Oro, J.L. Serrano, E. Sola, Coord. Chem. Rev. 117 (1992) 215.
[6] A.M. Giroud-Godquin, P.M. Maitlis, Angew. Chem. Int. Ed. Engl. 30 (1991) 375.
[7] D.W. Bruce, E. Lalinde, P. Styring, D.A. Dunmur, P.M. Maitlis, J. Chem. Soc. Chem. Commun. (1986) 581.
[8] M.A. Esteruelas, E. Sola, L.A. Oro, M.B. Ros, J.L. Serrano, J. Chem. Soc. Chem. Commun. (1989) 55.
[9] M.A. Esteruelas, E. Sola, L.A. Oro, M.B. Ros, M. Marcos, J.L. Serrano, J. Organomet. Chem. 387 (1990) 103.
[10] D.W. Bruce, D.A. Dunmur, M.A. Esteruelas, S.E. Hunt, R. Le Lagadec, P.M. Maitlis, J.R. Marsden, E. Sola, J.M. Stacey, J. Mater. Chem. 1 (1991) 251.
[11] H. Adams, N.A. Bailey, D.W. Bruce, S.A. Hudson, J.R. Marsden, Liq. Cryst. 16 (1994) 643.
[12] P. Berdagué, J. Courtieu, P.M. Maitlis, J. Chem. Soc. Chem. Commun. (1994) 1313.
[13] D.W. Bruce, M.D. Hall, Mol. Cryst. Liq. Cryst. 250 (1994) 373.
[14] J. Barberá, A. Elduque, R. Giménez, F.J. Lahoz, J.A. López, L.A. Oro, J.L. Serrano, B. Villacampa, J. Villalba, Inorg. Chem. 38 (1999) 3085.
[15] M. Cano, J.A. Campo, J.V. Heras, J. Lafuente, C. Rivas, E. Pinilla, Polyhedron 14 (1995) 1139.
[16] M.J. Decker, D.O. Kimberley Fjeldsted, S.R. Stobart, M.J. Zaworotko, J. Chem. Soc. Chem. Commun. (1983) 1525.
[17] N.A. Bailey, E. Coates, G.B. Robertson, F. Bonati, R. Ugo, Chem. Commun. (1967) 1041.
[18] C.G. Pitt, L.K. Monteith, L.F. Ballard, J.P. Collman, J.C. Morrow, W.R. Roper, D. Ulkü, J. Am. Chem. Soc. 88 (1966) 4286.
[19] M. Cano, J.V. Heras, M. Maeso, M. Alvaro, R. Fernández, E. Pinilla, J.A. Campo, A. Monge, J. Organomet. Chem. 534 (1997) 159.
[20] E.W. Abel, M.A. Bennet, G. Wilkinson, J. Chem. Soc. (1959) 3178.
[21] J. Chatt, L.M. Venanzi, J. Chem. Soc. (1957) 4735.
[22] K. Ohta, H. Muroki, K.I. Hatada, I. Yamamoto, K. Matsuzaki, Mol. Cryst. Liq. Cryst. 130 (1985) 249.
[23] G.M. Sheldrick, SHELXL97, Program for Refinement of Crystal Structure, University of Göttingen, Göttingen, Germany, 1997.
[24] S. Trofimenko, J.C. Calabrese, P.J. Domaille, J.S. Thompson, Inorg. Chem. 28 (1989) 1091.
[25] S. Trofimenko, J.C. Calabrese, J.K. Kochi, S. Wolowiec, F.B. Hulsbergen, J. Reedjik, Inorg. Chem. 31 (1992) 3943.
[26] S. Trofimenko, J.C. Calabrese, J.S. Thompson, Inorg. Chem. 26 (1987) 1507.
[27] F. Aguilar-Parrilla, C. Cativiela, M.D. Díaz de Villegas, J. Elguero, C. Foces-Foces, J.I. García-Laureiro, F. Hernández-

Cano, H.H. Limbach, J.A.S. Smith, C. Toiron, J. Chem. Soc. Perkin Trans. 2 (1992) 1737.
[28] M. Begtrup, G. Boyer, P. Cabildo, C. Cativiela, R.M. Claramunt, J. Elguero, J.I. García, C. Toiron, P. Vedsø, Magn. Reson. Chem. 31 (1993) 107.
[29] C. López, D. Sanz, R.M. Claramunt, S. Trofimenko, J. Elguero, J. Organomet. Chem. 503 (1995) 265.
[30] M. Cocivera, G. Ferguson, F.J. Lalor, P. Szczecinski, Organometallics 1 (1982) 1139.
[31] D. Carmona, J. Ferrer, M.P. Lamata, L.A. Oro, H.H. Limbach, G. Scherer, J. Elguero, M.L. Jimeno, J. Organomet. Chem. 470 (1994) 271.
[32] J.A. Campo, M. Cano, J.V. Heras, E. Pinilla, A. Monge, J.A. McCleverty, J. Chem. Soc. Dalton Trans. (1998) 3065.
[33] M.D. Santa María, R.M. Claramunt, J.A. Campo, M. Cano, R. Criado, J.V. Heras, P. Ovejero, E. Pinilla, M.R. Torres, J. Organomet. Chem. 605 (2000) 117.
[34] G. Aullón, S. Alvarez, Chem. Eur. J. 3 (1997) 655.
[35] D. Markovitsi, J. Andre, A. Mathis, J. Simon, P. Spegt, G. Weill, M. Ziliox, Chem. Phys. Lett. 104 (1984) 46.